43rd AIAA/ASME/SAE/ASEE Joint Propulsion Conference & Exhibit
8 - 11 July 2007, Cincinnati, OH

AIAA 2007-5808

Hydrodynamic Stability Analysis of Solid Rocket Motors with Arbitrary Grain Design

Jonathan C. French*
Software and Engineering Associates, Huntsville, AL 35670

and

Joseph Majdalani†
University of Tennessee Space Institute, Tullahoma, TN 37388

Solid rocket motor combustion stability analysis has historically focused on the linear acoustic stability problem. Acoustic instability presumes that the perturbed flowfield is irrotational and compressible. Recent efforts by Abu-Irshaid, Majdalani, and Casalis (Abu-Irshaid, E. M., Majdalani, J., and Casalis, G., "Hydrodynamic Stability of Rockets with Headwall Injection," *Physics of Fluids*, Vol. 19, No. 2, 2007, pp. 024101-11) and Chedevergne, Casalis and Majdalani (Chedevergne, F., Casalis, G., and Majdalani, J., "Biglobal Linear Stability Analysis and DNS Investigation of the Flow Induced by Wall Injection," AIAA Paper 2007-5796, July 2007) have demonstrated that hydrodynamic instability, based on a complementary rotational incompressible perturbed flowfield, can be incorporated into the linear stability analysis and significantly impact the predicted stability of large L/D solid rocket motors (SRMs). The intrinsic perturbed fluid motions connected with hydrodynamic instability can play a major role in inducing large acoustic and subsequent thrust oscillations in long segmented SRMs. As in acoustic stability analysis, hydrodynamic stability analysis requires the computation of mode shapes corresponding to the geometric shape of the motor cavity of interest. Software and Engineering Associates, Inc. (SEA) has presented several articles detailing the derivation and computation of acoustic mode shapes, and herein presents a similar approach and results for the computation of hydrodynamic mode shapes using the ARPACK eigensolver.

Nomenclature

a	=	chamber radius
A_i	=	inlet area
b	=	chamber discharge radius
l	=	chamber aspect ratio, L/a
P	=	normalized mean pressure, $\bar{P}/(\rho U_{inj}^2)$
p	=	normalized pressure amplitude, $\bar{p}/(\rho U_{inj}^2)$
$\bar{Q}_i$	=	inlet volumetric flow rate
Q_i	=	normalized volumetric flow rate, $\bar{Q}_i/(U_{inj}a^2) = \sigma^{-1}$
Re	=	injection Reynolds number, $U_{inj}a/\nu$
r	=	normalized radial coordinate, $\bar{r}/a$
S	=	swirl number, $\pi ab/A_i = \pi\sigma/\sqrt{2}$
u	=	normalized velocity amplitude $(\bar{u}_r, \bar{u}_z, \bar{u}_\theta)/U_{inj}$
U	=	normalized mean inflow velocity, $\left(\bar{U}_r, \bar{U}_\theta, \bar{U}_z\right)/U_{inj}$
$\bar{U}_{inj}$	=	tangential injection velocity $\bar{Q}_i/A_i$

*Huntsville Operations Manager. Member AIAA.

†Jack D. Whitfield Professor of High Speed Flows, Department of Mechanical, Aerospace and Biomedical Engineering. Member AIAA. Fellow ASME.

Copyright © 2007 by Software and Engineering Associates, Inc. Published by the American Institute of Aeronautics and Astronautics, Inc., with permission.

V = vortex Reynolds number, $Q_i Re(a/L)$
z = normalized axial coordinate, $\bar{z}/a$

Greek
β = normalized discharge radius, b/a
κ = inflow parameter, $Q_i/(2\pi l) = (2\pi\sigma l)^{-1}$
ν = kinematic viscosity, μ/ρ
ρ = density
σ = modified swirl number, $Q_i^{-1} = S\sqrt{2}/\pi$

Subscripts
i = inlet property
r = radial component or partial derivative
z = axial component or partial derivative
$\underline{\theta}$ = azimuthal component or partial derivative
= overbars denote dimensional variables
~ = denotes total (instantaneous) quantities
^ = denotes fluctuating quantities

I. Introduction

THE purpose of this study is to develop a hydrodynamic stability analysis tool to assist in the design of rocket motors. Unlike acoustic instability, hydrodynamic instability is driven by disturbances emanating from the mean flow itself, and tools need to be developed to evaluate this potential problem within the design cycle.

The hydrodynamic instability waves are different from acoustic waves in that they exhibit short wavelengths and slow propagation speeds that vary spatially, while the vortico-acoustic waves exhibit large wavelengths and propagation speeds that are comparable to the speed of sound. By recognizing that the hydrodynamic and acoustic disturbance modes evolve over vastly dissimilar spatial and temporal scales, their effects can be superimposed.

In recent work by Chedevergne *et al.*,[1-4] it was demonstrated that when hydrodynamic instability eigenmodes fall close to acoustic frequencies, a lock-on mechanism takes place leading to resonant-like interactions. The so-called intrinsic (i.e. hydrodynamic) instability modes couple with the acoustic modes to the extent of triggering appreciable steep fronted acoustic waves, resulting in large thrust oscillations. Such behavior was not only predicted through stability theory, but also confirmed in live subscale firings, extrapolated from cold flow experiments, and captured with DNS simulations. Furthermore, recent investigations by Abu-Irshaid, Majdalani and Casalis,[5] and Bhatia *et al.*[6] have demonstrated the possibility of evaluating hydrodynamic instability contributions to the total unsteady energy in a rocket motor. Through the present work, the analytic models developed by Abu-Irshaid, Majdalani and Casalis,[5] Bhatia *et al.*,[6] and Chedevergne *et al.*[1-4] will be implemented in an improved combustion instability framework originating from the efforts of Flandro *et al.*[7,8]

The need to incorporate hydrodynamic instability waves in combustion instability computations has been recently emphasized by Casalis and co-workers, particularly by Chedevergne *et al.*,[1-4] Griffond and Casalis,[9,10] Griffond,[11] Féraille and Casalis,[12] and others. The importance of accounting for unsteady vorticity in general has been emphasized by Fischbach *et al.*,[13-16] Flandro *et al.*,[7,8] Flandro and Majdalani,[17] Majdalani *et al.*,[18-29] Balachandar *et al.*,[30] Wasistho *et al.*,[31] and others.[32-34] Our chief purpose will be to extend and implement their techniques in a general 3D capable linear stability tool that has been under development by French *et al.*[35-38] In the process, the interactions between the perturbed acoustic and hydrodynamic flowfields will be elucidated and their added energy will be computed for arbitrary grain geometry.

The development of this tool enhances the design of combustion devices by avoiding costly prototype remanufacture. This is accomplished through reliance on numerical prediction of combustion stability characteristics during early SRM design stages. Currently, many large solid rocket motors exhibit hydrodynamic stability problems, including the Shuttle RSRM, Titan, and the Ariane V.[39] It is expected that the RSRM-V will also be susceptible to hydrodynamic instability. In fact, according to established analysis, hydrodynamic instability effects become more pronounced in longer rocket chambers. Furthermore, recent studies by Chedevergne, Casalis and Majdalani[1] have identified a major source of large thrust oscillations to be connected with the coupling between hydrodynamic instability and acoustic frequencies. By avoiding stability issues in the design process, our analysis

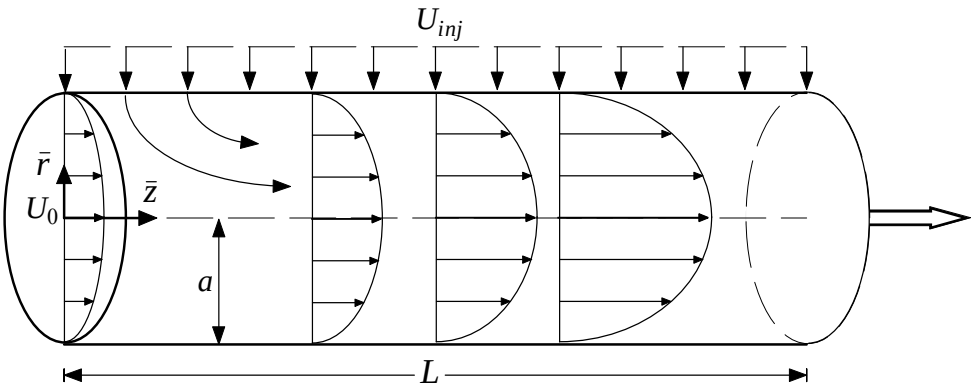

a) Internal burning chamber model for an internal burning SRM (Solid Rocket Motor)

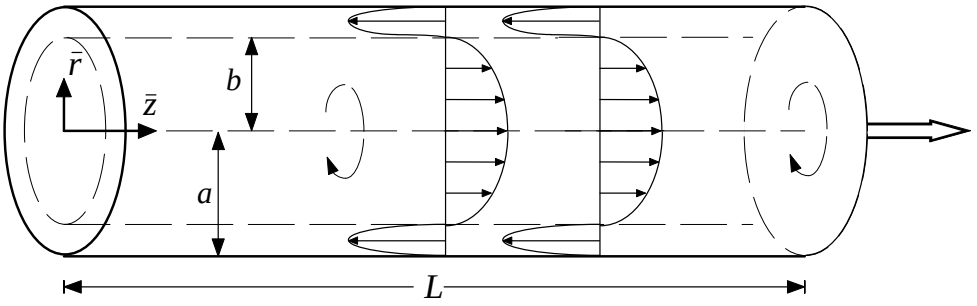

b) Bidirectional vortex chamber model for a VCCWC (Vortex Combustion Cold-Wall Chamber)

Figure 1. Sketches of chamber cavities for two basic flow models.

has the potential to not only save on revenue and loss in momentum, but also prevent developmental programs from being cancelled due to design problems arising late in the process.

The first numerical study of hydrodynamic instability in an SRM model was carried out by Varapaev and Yagodkin.[40] This was followed by several studies on flowfield instability and turbulence by Beddini,[41] Beddini and Roberts,[42,43] and Lee and Beddini.[44,45] Totally independently, an extended investigation that included laboratory measurements and full solutions of the Navier-Stokes equations was performed by Casalis and co-workers.[9,46] Their work helped to explain the effects of radial disturbances and the inconsistencies between the two available techniques, namely, the one that relied on perturbing the primitive variables versus the one that employed the stream function approach.[41,42] Other related studies that may be useful to report fall under two general categories: first, those on the unsteady wave characteristics in solid rocket motors (e.g., Avalon and Comas,[47] and Vuillot and Avalon[48]); and, second, those on parietal vortex shedding and its connection to hydrodynamic instability (Vuillot,[49] Couton *et al.*,[50] Ugurtas *et al.*, [51] and Avalon *et al.*[52]). In this regard, two excellent surveys may be found in Ugurtas *et al.*[53] and Fabignon *et al.*[54]

In similar context, the purpose of the present analysis is to implement the latest results obtained, respectively, by Abu-Irshaid, Majdalani and Casalis,[5] and Bhatia *et al.*[6] in the global evaluation scheme of rocket combustion instability. As in acoustic analysis, hydrodynamic instability analysis requires the computation of mode shapes corresponding to particular rocket chamber geometry. The authors have presented several papers detailing the derivation and computation of acoustic mode shapes, and herein present a similar approach and results for the computation of hydrodynamic mode shapes using the ARPACK eigensolver.[55] While this paper repeats the computation of [5] in 1-D, the purpose of this exercise is to demonstrate that the problem can be solved using the ARPACK eigensolver, and in doing so demonstrate the feasibility of using this numerical approach to solve for the 3-D hydrodynamic stability modes.

II. Formulation

A. Basic Flow Geometry

The basic rocket chamber can be modeled as a porous cylinder of length L and radius a. We also permit the forward end to be porous while assuming an open aft end. As shown in Fig. 1, $\bar{r}$ and $\bar{z}$ stand for the radial and axial coordinates. In Fig. 1a, the porous headwall permits the injection of a fluid at a prescribed velocity profile, $\bar{u}_0$. For example, using a similarity conforming Berman profile, one can take $\bar{u}_0 = U_0 \cos(\frac{1}{2}\pi \bar{r}^2 / a^2)$. For the bidirectional vortex chamber (Fig. 1b), the headwall is closed to permit the axial reversal in cyclonic flow motion. For both models depicted in Fig. 1, our solution domain extends from the headwall to the parallel, virtual nozzle attachment plane at the aft end. Beginning with the incompressible Navier-Stokes system of equations for a cylindrical cavity, we follow Abu-Irshaid, Majdalani and Casalis[56] and write the fundamental equations.

B. Fundamental Equations

Continuity:

$$\frac{\partial \tilde{U}_r}{\partial r} + \frac{\tilde{U}_r}{r} + \frac{1}{r}\frac{\partial \tilde{U}_\theta}{\partial \theta} + \frac{\partial \tilde{U}_z}{\partial z} = 0 \tag{1}$$

r-Momentum:

$$\frac{\partial \tilde{U}_r}{\partial t} + \tilde{U}_r \frac{\partial \tilde{U}_r}{\partial r} + \frac{\tilde{U}_\theta}{r}\frac{\partial \tilde{U}_r}{\partial \theta} - \frac{\tilde{U}_\theta^2}{r} + \tilde{U}_z \frac{\partial \tilde{U}_r}{\partial z} + \frac{\partial P}{\partial r} = \frac{1}{Re}\left(\frac{\partial^2 \tilde{U}_r}{\partial r^2} + \frac{1}{r}\frac{\partial \tilde{U}_r}{\partial r} - \frac{\tilde{U}_r}{r^2} + \frac{1}{r^2}\frac{\partial^2 \tilde{U}_r}{\partial \theta^2} - \frac{2}{r^2}\frac{\partial \tilde{U}_\theta}{\partial \theta} + \frac{\partial^2 \tilde{U}_r}{\partial z^2} \right) \tag{2}$$

θ-Momentum:

$$\frac{\partial \tilde{U}_\theta}{\partial t} + \tilde{U}_r \frac{\partial \tilde{U}_\theta}{\partial r} + \frac{\tilde{U}_\theta}{r}\frac{\partial \tilde{U}_\theta}{\partial \theta} + \frac{\tilde{U}_r \tilde{U}_\theta}{r} + \tilde{U}_z \frac{\partial \tilde{U}_\theta}{\partial z} + \frac{1}{r}\frac{\partial P}{\partial \theta} = \frac{1}{Re}\left(\frac{\partial^2 \tilde{U}_\theta}{\partial r^2} + \frac{1}{r}\frac{\partial \tilde{U}_\theta}{\partial r} - \frac{\tilde{U}_\theta}{r^2} + \frac{1}{r^2}\frac{\partial^2 \tilde{U}_\theta}{\partial \theta^2} + \frac{2}{r^2}\frac{\partial \tilde{U}_r}{\partial \theta} + \frac{\partial^2 \tilde{U}_\theta}{\partial z^2} \right) \tag{3}$$

z-Momentum:

$$\frac{\partial \tilde{U}_z}{\partial t} + \tilde{U}_r \frac{\partial \tilde{U}_z}{\partial r} + \frac{\tilde{U}_\theta}{r}\frac{\partial \tilde{U}_z}{\partial \theta} + \tilde{U}_z \frac{\partial \tilde{U}_z}{\partial z} + \frac{\partial P}{\partial z} = \frac{1}{Re}\left(\frac{\partial^2 \tilde{U}_z}{\partial r^2} + \frac{1}{r}\frac{\partial \tilde{U}_z}{\partial r} + \frac{1}{r^2}\frac{\partial^2 \tilde{U}_z}{\partial \theta^2} + \frac{\partial^2 \tilde{U}_z}{\partial z^2} \right) \tag{4}$$

where $Re = U_{inj} a / \nu$ represents the Reynolds number based on the injection velocity, either sidewall or circumferential, as shown in Figs. 1a and b. Then each instantaneous variable $\tilde{U}$ is decomposed into a mean U and a fluctuating part $\breve{u}$. When substituted in the above, one collects:

Continuity:

$$\frac{\partial (U_r + \breve{u}_r)}{\partial r} + \frac{(U_r + \breve{u}_r)}{r} + \frac{1}{r}\frac{\partial (U_\theta + \breve{u}_\theta)}{\partial \theta} + \frac{\partial (U_z + \breve{u}_z)}{\partial z} = 0 \quad \text{or} \quad \begin{cases} \dfrac{\partial U_r}{\partial r} + \dfrac{U_r}{r} + \dfrac{1}{r}\dfrac{\partial U_\theta}{\partial \theta} + \dfrac{\partial U_z}{\partial z} = 0 \\ \dfrac{\partial \breve{u}_r}{\partial r} + \dfrac{\breve{u}_r}{r} + \dfrac{1}{r}\dfrac{\partial \breve{u}_\theta}{\partial \theta} + \dfrac{\partial \breve{u}_z}{\partial z} = 0 \end{cases} \tag{5}$$

r-Momentum:

$$\begin{cases} \dfrac{\partial U_r}{\partial t} + U_r \dfrac{\partial U_r}{\partial r} + \dfrac{U_\theta}{r}\dfrac{\partial U_r}{\partial \theta} - \dfrac{U_\theta^2}{r} + U_z \dfrac{\partial U_r}{\partial z} + \dfrac{\partial P}{\partial r} = \dfrac{1}{Re}\left(\dfrac{\partial^2 U_r}{\partial r^2} + \dfrac{1}{r}\dfrac{\partial U_r}{\partial r} - \dfrac{U_r}{r^2} + \dfrac{1}{r^2}\dfrac{\partial^2 U_r}{\partial \theta^2} - \dfrac{2}{r^2}\dfrac{\partial U_\theta}{\partial \theta} + \dfrac{\partial^2 U_r}{\partial z^2} \right) \\ \dfrac{\partial \breve{u}_r}{\partial t} + U_r \dfrac{\partial \breve{u}_r}{\partial r} + \breve{u}_r \dfrac{\partial U_r}{\partial r} + \dfrac{U_\theta}{r}\dfrac{\partial \breve{u}_r}{\partial \theta} + \dfrac{\breve{u}_\theta}{r}\dfrac{\partial U_r}{\partial \theta} - \dfrac{2U_\theta \breve{u}_\theta}{r} + U_z \dfrac{\partial \breve{u}_r}{\partial z} + \breve{u}_z \dfrac{\partial U_r}{\partial z} + \dfrac{\partial \breve{p}}{\partial r} \\ \qquad = \dfrac{1}{Re}\left(\dfrac{\partial^2 \breve{u}_r}{\partial r^2} + \dfrac{1}{r}\dfrac{\partial \breve{u}_r}{\partial r} - \dfrac{\breve{u}_r}{r^2} + \dfrac{1}{r^2}\dfrac{\partial^2 \breve{u}_r}{\partial \theta^2} - \dfrac{2}{r^2}\dfrac{\partial \breve{u}_\theta}{\partial \theta} + \dfrac{\partial^2 \breve{u}_r}{\partial z^2} \right) \end{cases} \tag{6}$$

θ-Momentum:

$$\begin{cases} \dfrac{\partial U_\theta}{\partial t}+U_r\dfrac{\partial U_\theta}{\partial r}+\dfrac{U_\theta}{r}\dfrac{\partial U_\theta}{\partial \theta}+\dfrac{U_rU_\theta}{r}+\tilde{U}_z\dfrac{\partial U_\theta}{\partial z}+\dfrac{1}{r}\dfrac{\partial P}{\partial \theta}=\dfrac{1}{Re}\left(\dfrac{\partial^2 U_\theta}{\partial r^2}+\dfrac{1}{r}\dfrac{\partial U_\theta}{\partial r}-\dfrac{U_\theta}{r^2}+\dfrac{1}{r^2}\dfrac{\partial^2 U_\theta}{\partial \theta^2}+\dfrac{2}{r^2}\dfrac{\partial U_r}{\partial \theta}+\dfrac{\partial^2 U_\theta}{\partial z^2}\right) \\ \dfrac{\partial \breve{u}_\theta}{\partial t}+U_r\dfrac{\partial \breve{u}_\theta}{\partial r}+\breve{u}_r\dfrac{\partial U_\theta}{\partial r}+\dfrac{U_\theta}{r}\dfrac{\partial \breve{u}_\theta}{\partial \theta}+\dfrac{\breve{u}_\theta}{r}\dfrac{\partial U_\theta}{\partial \theta}+\dfrac{U_r\breve{u}_\theta}{r}+\dfrac{\breve{u}_rU_\theta}{r}+U_z\dfrac{\partial \breve{u}_\theta}{\partial z}+\breve{u}_z\dfrac{\partial U_\theta}{\partial z}+\dfrac{1}{r}\dfrac{\partial \breve{p}}{\partial \theta} \\ \qquad =\dfrac{1}{Re}\left(\dfrac{\partial^2 \breve{u}_\theta}{\partial r^2}+\dfrac{1}{r}\dfrac{\partial \breve{u}_\theta}{\partial r}-\dfrac{\breve{u}_\theta}{r^2}+\dfrac{1}{r^2}\dfrac{\partial^2 \breve{u}_\theta}{\partial \theta^2}+\dfrac{2}{r^2}\dfrac{\partial \breve{u}_r}{\partial \theta}+\dfrac{\partial^2 \breve{u}_\theta}{\partial z^2}\right) \end{cases} \tag{7}$$

z-Momentum:

$$\begin{cases} \dfrac{\partial U_z}{\partial t}+U_r\dfrac{\partial U_z}{\partial r}+\dfrac{\left(U_\theta+\breve{u}_\theta\right)}{r}\dfrac{\partial U_z}{\partial \theta}+U_z\dfrac{\partial U_z}{\partial z}+\dfrac{\partial P}{\partial z}=\dfrac{1}{Re}\left(\dfrac{\partial^2 U_z}{\partial r^2}+\dfrac{1}{r}\dfrac{\partial U_z}{\partial r}+\dfrac{1}{r^2}\dfrac{\partial^2 U_z}{\partial \theta^2}+\dfrac{\partial^2 U_z}{\partial z^2}\right) \\ \dfrac{\partial \breve{u}_z}{\partial t}+U_r\dfrac{\partial \breve{u}_z}{\partial r}+\breve{u}_r\dfrac{\partial U_z}{\partial r}+\dfrac{U_\theta}{r}\dfrac{\partial \breve{u}_z}{\partial \theta}+\dfrac{\breve{u}_\theta}{r}\dfrac{\partial U_z}{\partial \theta}+U_z\dfrac{\partial \breve{u}_z}{\partial z}+\breve{u}_z\dfrac{\partial U_z}{\partial z}+\dfrac{\partial \breve{p}}{\partial z}=\dfrac{1}{Re}\left(\dfrac{\partial^2 \breve{u}_z}{\partial r^2}+\dfrac{1}{r}\dfrac{\partial \breve{u}_z}{\partial r}+\dfrac{1}{r^2}\dfrac{\partial^2 \breve{u}_z}{\partial \theta^2}+\dfrac{\partial^2 \breve{u}_z}{\partial z^2}\right) \end{cases} \tag{8}$$

C. Normal Mode Fluctuations

Using the normal mode approach, we impose fluctuations that exhibit an exponential dependence on z and an arbitrary radial dependence of the type:

$$\begin{cases} \breve{u}_r=u_r(r)\exp\left[i\left(q\theta+\sigma z-\omega t\right)\right] & \breve{u}_\theta=u_\theta(r)\exp\left[i\left(q\theta+\sigma z-\omega t\right)\right] \\ \breve{u}_z=u_z(r)\exp\left[i\left(q\theta+\sigma z-\omega t\right)\right] & \breve{p}=p(r)\exp\left[i\left(q\theta+\sigma z-\omega t\right)\right] \end{cases} \tag{9}$$

Continuity:

$$\frac{\partial \breve{u}_r}{\partial r}+\frac{\breve{u}_r}{r}+\frac{1}{r}\frac{\partial \breve{u}_\theta}{\partial \theta}+\frac{\partial \breve{u}_z}{\partial z}=0 \quad \text{or} \quad \frac{\partial u_r}{\partial r}+\frac{1}{r}u_r+\frac{iq}{r}u_\theta+i\sigma u_z=0 \tag{10}$$

r-Momentum:

$$\left[-i\omega+\frac{\partial U_r}{\partial r}+\frac{iqU_\theta}{r}+\frac{1}{r}\frac{\partial U_r}{\partial \theta}+i\sigma U_z+\frac{1}{Re}\left(\frac{1}{r^2}+\frac{q^2}{r^2}+\sigma^2\right)\right]u_r$$
$$+\left(\frac{1}{Re}\frac{2iq}{r^2}-\frac{2U_\theta}{r}\right)u_\theta+\frac{\partial U_r}{\partial z}u_z+\frac{\partial p}{\partial r}+\left(U_r-\frac{1}{Re}\frac{1}{r}\right)\frac{\partial u_r}{\partial r}-\frac{1}{Re}\frac{\partial^2 u_r}{\partial r^2}=0 \tag{11}$$

θ-Momentum:

$$\left(\frac{\partial U_\theta}{\partial r}+\frac{U_\theta}{r}-\frac{1}{Re}\frac{2iq}{r^2}\right)u_r+\left[-i\omega+iq\frac{U_\theta}{r}+\frac{1}{r}\frac{\partial U_\theta}{\partial \theta}+\frac{U_r}{r}+i\sigma U_z+\frac{1}{Re}\left(\frac{1}{r^2}+\frac{q^2}{r^2}+\sigma^2\right)\right]u_\theta$$
$$+\frac{\partial U_\theta}{\partial z}u_z+\frac{iq}{r}p+\left(U_r-\frac{1}{Re}\frac{1}{r}\right)\frac{\partial u_\theta}{\partial r}-\frac{1}{Re}\frac{\partial^2 u_\theta}{\partial r^2}=0 \tag{12}$$

z-Momentum:

$$\frac{\partial U_z}{\partial r}u_r+\frac{1}{r}\frac{\partial U_z}{\partial \theta}u_\theta+\left[-i\omega+\frac{iqU_\theta}{r}+i\sigma U_z+\frac{\partial U_z}{\partial z}+\frac{1}{Re}\left(\frac{q^2}{r^2}+\sigma^2\right)\right]u_z+i\sigma p+\left(U_r-\frac{1}{Re}\frac{1}{r}\right)\frac{\partial u_z}{\partial r}-\frac{1}{Re}\frac{\partial^2 u_z}{\partial r^2}=0 \tag{13}$$

D. Interaction Equations for the Vyas-Majdalani Mean Flow Model

In order to evaluate the temporal instability of the bidirectional vortex we select the solution obtained by Vyas, Majdalani and Chiaverini[57] (see Fig. 1b). This is described by:

$$\begin{cases} U_r = -\kappa \dfrac{1}{r}\sin\left(\pi r^2\right) \\ U_\theta = \dfrac{1-e^{-Vr^2/4}}{r\left(1-e^{-V/4}\right)} \\ U_z = 2\pi\kappa z\cos\left(\pi r^2\right) \end{cases} \tag{14}$$

where in relation to the modified swirl number σ, the vortex Reynolds number is given by

$$V = 2\pi\kappa Re = \frac{Re}{\sigma}\frac{a}{L} \tag{15}$$

Based on Eq. (14), the following simplifications are in order:

$$\frac{\partial U_r}{d\theta} = \frac{\partial U_r}{dz} = \frac{\partial U_\theta}{d\theta} = \frac{\partial U_\theta}{dz} = \frac{\partial U_z}{d\theta} = 0 \tag{16}$$

When inserted into the interaction equations, they lead to:

r-Momentum:

$$\left[-i\omega + \frac{\partial U_r}{\partial r} + \frac{iqU_\theta}{r} + i\sigma U_z + \frac{1}{Re}\left(\frac{1}{r^2} + \frac{q^2}{r^2} + \sigma^2\right)\right]u_r + \left(\frac{1}{Re}\frac{2iq}{r^2} - \frac{2U_\theta}{r}\right)u_\theta + 0u_z$$

$$+\frac{\partial p}{\partial r} + \left(U_r - \frac{1}{Re}\frac{1}{r}\right)\frac{\partial u_r}{\partial r} - \frac{1}{Re}\frac{\partial^2 u_r}{\partial r^2} = 0 \tag{17}$$

θ-Momentum:

$$\left(\frac{\partial U_\theta}{\partial r} + \frac{U_\theta}{r} - \frac{1}{Re}\frac{2iq}{r^2}\right)u_r + \left[-i\omega + iq\frac{U_\theta}{r} + \frac{U_r}{r} + i\sigma U_z + \frac{1}{Re}\left(\frac{1}{r^2} + \frac{q^2}{r^2} + \sigma^2\right)\right]u_\theta + 0u_z$$

$$+\frac{iq}{r}p + \left(U_r - \frac{1}{Re}\frac{1}{r}\right)\frac{\partial u_\theta}{\partial r} - \frac{1}{Re}\frac{\partial^2 u_\theta}{\partial r^2} = 0 \tag{18}$$

z-Momentum:

$$\frac{\partial U_z}{\partial r}u_r + 0u_\theta + \left[-i\omega + \frac{iqU_\theta}{r} + i\sigma U_z + \frac{\partial U_z}{\partial z} + \frac{1}{Re}\left(\frac{q^2}{r^2} + \sigma^2\right)\right]u_z + i\sigma p + \left(U_r - \frac{1}{Re}\frac{1}{r}\right)\frac{\partial u_z}{\partial r} - \frac{1}{Re}\frac{\partial^2 u_z}{\partial r^2} = 0 \tag{19}$$

Further simplifications may be realized by substituting the analytical derivatives of the mean flow. These are

$$\frac{\mathrm{d}U_r}{\mathrm{d}r} = -\kappa\left[-\frac{1}{r^2}\sin\left(\pi r^2\right) + \frac{1}{r}\cos\left(\pi r^2\right)2\pi r\right] = \kappa\left[\frac{1}{r^2}\sin\left(\pi r^2\right) - 2\pi\cos\left(\pi r^2\right)\right] \tag{20}$$

$$\frac{\mathrm{d}U_\theta}{\mathrm{d}r} = \frac{1}{\left(1-e^{-\pi\kappa Re/2}\right)}\left[\left(\pi\kappa Re + \frac{1}{r^2}\right)e^{-\pi\kappa Rer^2/2} - \frac{1}{r^2}\right] \tag{21}$$

Then defining

$$f = -\pi\kappa Re/2 \quad V = 2\pi\kappa Re = -4f \tag{22}$$

One has

$$U_\theta = \frac{1-e^{fr^2}}{r\left(1-e^{f}\right)} = \frac{1-e^{-\pi\kappa Rer^2/2}}{r\left(1-e^{-\pi\kappa Re/2}\right)} \qquad \frac{\mathrm{d}U_\theta}{\mathrm{d}r} = \frac{1}{\left(1-e^{f}\right)}\left[\left(\frac{1}{r^2}-2f\right)e^{fr^2} - \frac{1}{r^2}\right] \tag{23}$$

Lastly,

$$\frac{\mathrm{d}U_z}{\mathrm{d}r} = -4\pi^2\kappa rz\sin\left(\pi r^2\right) \qquad \frac{\mathrm{d}U_z}{\mathrm{d}z} = 2\pi\kappa\cos\left(\pi r^2\right) \tag{24}$$

III. Discretization

For this analysis, z is a fixed location and the only spatially varying parameter is the mean flow radial parameter. As we are given a functional form of the spatially varying mean flow we will include this variation analytically in the discretization by using a two function Taylor series expansion, presuming we know the function "g":

$$\begin{aligned} g(r+h)F(r+h) = {} & g(r)F(r) + \Delta r\left[g(r)F(r)\right]_r + \tfrac{1}{2}\Delta r^2\left[g(r)F(r)\right]_{rr} \\ & + \tfrac{1}{6}\Delta r^3\left[g(r)F(r)\right]_{rrr} + \tfrac{1}{24}\Delta r^4\left[g(r)F(r)\right]_{rrrr} + O\left(\Delta r^5\right) \end{aligned} \tag{25}$$

Then letting $h \equiv \Delta r$, we have

$$\begin{cases} g(r+h)F(r+h) = gF + h\left[g_rF + gF_r\right] + \tfrac{1}{2}h^2\left[gF\right]_{rr} + \tfrac{1}{6}h^3\left[gF\right]_{rrr} + \tfrac{1}{24}h^4\left[gF\right]_{rrrr} + O\left(h^5\right) \\ g(r-h)F(r-h) = gF - h\left[g_rF + gF_r\right] + \tfrac{1}{2}h^2\left[gF\right]_{rr} - \tfrac{1}{6}h^3\left[gF\right]_{rrr} + \tfrac{1}{24}h^4\left[gF\right]_{rrrr} + O\left(h^5\right) \end{cases} \tag{26}$$

Subtracting, we get

$$g(r+h)F(r+h) - g(r-h)F(r-h) = 2h\left[g_rF + gF_r\right] + \tfrac{1}{3}h^3\left[gF\right]_{rrr} + O\left(h^4\right) \tag{27}$$

Then solving for gF_r , we retrieve

$$\begin{cases} gF_r = \dfrac{1}{2h}\left[g(r+h)F(r+h) - g(r-h)F(r-h)\right] - g_r(r)F(r) + O\left(h^2\right) \\ gF_r = \left(gF\right)_r - g_rF \end{cases} \tag{28}$$

Similarly

$$\begin{aligned} g(r+h)F(r+h) = {} & g(r)F(r) + h\left[g(r)F(r)\right]_r + \tfrac{1}{2}h^2\left[g(r)F(r)\right]_{rr} \\ & + \tfrac{1}{6}h^3\left[g(r)F(r)\right]_{rrr} + \tfrac{1}{24}h^4\left[g(r)F(r)\right]_{rrrr} + O\left(h^5\right) \end{aligned} \tag{29}$$

and so

$$g(r+h)F(r+h) = gF + h\left[gF\right]_r + \tfrac{1}{2}h^2\left[g_{rr}F + 2g_rF_r + gF_{rr}\right] + \tfrac{1}{6}h^3\left[gF\right]_{rrr} + \tfrac{1}{24}h^4\left[gF\right]_{rrrr} + O\left(h^5\right) \tag{30}$$

$$g(r-h)F(r-h) = gF - h\left[gF\right]_r + \tfrac{1}{2}h^2\left[g_{rr}F + 2g_rF_r + gF_{rr}\right] - \tfrac{1}{6}h^3\left[gF\right]_{rrr} + \tfrac{1}{24}h^4\left[gF\right]_{rrrr} + O\left(h^5\right) \tag{31}$$

When combined, these relations yield

$$g(r+h)F(r+h) + g(r-h)F(r-h) = 2gF + h^2\left[g_{rr}F + 2g_rF_r + gF_{rr}\right] + O\left(h^4\right) \tag{32}$$

This enables us to extract

$$gF_{rr} = \frac{1}{h^2}\left[g(r+h)F(r+h) - 2g(r)F(r) + g(r-h)F(r-h)\right] - g_{rr}F - 2g_rF_r + O\left(h^2\right) \tag{33}$$

$$\begin{cases} gF_r = (gF)_r - g_r F \\ g_r F_r = (g_r F)_r - g_{rr} F \end{cases} \tag{34}$$

and

$$\begin{cases} gF_{rr} = \dfrac{1}{h^2}\left[g(r+h)F(r+h) - 2g(r)F(r) + g(r-h)F(r-h)\right] - g_{rr}F - 2\left((g_r F)_r - g_{rr}F\right) + O\left(h^2\right) \\ gF_{rr} = \dfrac{1}{h^2}\left[g(r+h)F(r+h) - 2g(r)F(r) + g(r-h)F(r-h)\right] + g_{rr}F - 2(g_r F)_r + O\left(h^2\right) \\ gF_{rr} = (gF)_{rr} + g_{rr}F - 2(g_r F)_r \end{cases} \tag{35}$$

With the use of some of these expressions, we discretize the unsteady flow components to get

Continuity:

$$\begin{cases} r\dfrac{\partial u_r}{\partial r} + u_r + iqu_\theta + ir\sigma u_z = 0 \\ \dfrac{1}{2\Delta r}\left(r^{i+1}u_r^{i+1} - r^{i-1}u_r^{i-1}\right) + iqu_\theta^i + ir^i\sigma u_z^i = 0 \end{cases} \tag{36}$$

r-Momentum:

We first remove the singularity at the centerline by multiplying through by *r*:

$$\left[-i\omega r + r\frac{\partial U_r}{\partial r} + iqU_\theta + i\sigma rU_z + \frac{1}{Re}\left(\frac{1+q^2}{r} + r\sigma^2\right)\right]u_r + 2\left(\frac{iq}{rRe} - U_\theta\right)u_\theta + 0u_z$$

$$+ r\frac{\partial p}{\partial r} + \left(rU_r - \frac{1}{Re}\right)\frac{\partial u_r}{\partial r} - \frac{r}{Re}\frac{\partial^2 u_r}{\partial r^2} = 0 \tag{37}$$

Then applying a 2nd order Taylor series discretization with variable coefficients, we have

$$\left\{\left[-i\omega r + r\frac{\partial U_r}{\partial r} + iqU_\theta + i\sigma rU_z + \frac{1}{Re}\left(\frac{1+q^2}{r} + r\sigma^2\right)\right]u_r\right\}^i + \left[2\left(\frac{iq}{rRe} - U_\theta\right)u_\theta\right]^i$$

$$+0u_z + \frac{\Delta_{i-1}^{i+1}}{2\Delta r}(pr) - \left[p\frac{\mathrm{d}}{\mathrm{d}r}(r)\right]^i + \frac{\Delta_{i-1}^{i+1}}{2\Delta r}\left[\left(rU_r - \frac{1}{Re}\right)u_r\right] - \left[\frac{\mathrm{d}}{\mathrm{d}r}\left(rU_r - \frac{1}{Re}\right)u_r\right]^i$$

$$-\frac{1}{Re}\left\{\frac{\nabla_{i-1}^{i+1}}{(\Delta r)^2}(ru_r) + \left[\frac{\mathrm{d}^2}{\mathrm{d}r^2}(r)u_r\right]^i - 2\frac{\Delta_{i-1}^{i+1}}{2\Delta r}\left[\frac{\mathrm{d}}{\mathrm{d}r}(r)u_r\right]\right\} = 0 \tag{38}$$

Inserting the mean flow, simplifying the derivatives, and collecting by nodes, we retrieve

$$\left(\left\{\frac{1}{2\Delta r}\left[\kappa\sin\left(\pi r^2\right) - \frac{1}{Re}\right] - \frac{1}{Re}\frac{r}{(\Delta r)^2}\right\}u_r + 0u_\theta + 0u_z - \frac{pr}{2\Delta r}\right)^{i-1}$$

$$+\left(\begin{array}{l}\left\{-i\omega r + \kappa\dfrac{\sin\left(\pi r^2\right)}{r} + iq\dfrac{1-e^{-\pi\kappa Rer^2/2}}{r\left(1-e^{-\pi\kappa Re/2}\right)} + 2i\sigma r\pi\kappa z\cos\left(\pi r^2\right) + \dfrac{1}{Re}\left[\dfrac{1+q^2}{r} + r\sigma^2 + \dfrac{2r}{(\Delta r)^2}\right]\right\}u_r \\ +2\left[\dfrac{iq}{rRe} - \dfrac{1-e^{-\pi\kappa Rer^2/2}}{r\left(1-e^{-\pi\kappa Re/2}\right)}\right]u_\theta + 0u_z - p\end{array}\right)^i$$

$$+\left[\left\{\frac{1}{2\Delta r}\left[\frac{1}{Re}-\kappa\sin\left(\pi r^2\right)\right]-\frac{1}{Re}\frac{r}{\left(\Delta r\right)^2}\right\}u_r+0u_\theta+0u_z+\frac{pr}{2\Delta r}\right]^{i+1}=0 \tag{39}$$

θ-Momentum:

We remove the singularity at the centerline by multiplying through by *r:*

$$\left(r\frac{\partial U_\theta}{\partial r}+U_\theta-\frac{2iq}{rRe}\right)u_r+\left[-i\omega r+iqU_\theta+U_r+i\sigma rU_z+\frac{1}{Re}\left(\frac{1+q^2}{r}+r\sigma^2\right)\right]u_\theta$$

$$+0u_z+iqp+\left(rU_r-\frac{1}{Re}\right)\frac{\partial u_\theta}{\partial r}-\frac{r}{Re}\frac{\partial^2 u_\theta}{\partial r^2}=0 \tag{40}$$

As before, we use 2nd order Taylor series discretization with variable coefficients:

$$\left\{\left(r\frac{\partial U_\theta}{\partial r}+U_\theta-\frac{2iq}{rRe}\right)u_r\right\}^i+\left\{\left[-i\omega r+iqU_\theta+U_r+i\sigma rU_z+\frac{1}{Re}\left(\frac{1+q^2}{r}+r\sigma^2\right)\right]u_\theta\right\}^i$$

$$+0u_z+iq\left(p\right)^i+\frac{\Delta_{i-1}^{i+1}}{2\Delta r}\left[\left(rU_r-\frac{1}{Re}\right)u_\theta\right]-\left[\frac{\partial}{\partial r}\left(rU_r-\frac{1}{Re}\right)u_\theta\right]^i$$

$$-\frac{1}{Re}\left\{\frac{\nabla_{i-1}^{i+1}}{\left(\Delta r\right)^2}\left(ru_\theta\right)+\left[\frac{\mathrm{d}^2}{\mathrm{d}r^2}\left(r\right)u_\theta\right]^i-2\frac{\Delta_{i-1}^{i+1}}{2\Delta r}\left[\frac{\mathrm{d}}{\mathrm{d}r}\left(r\right)u_\theta\right]\right\}=0 \tag{41}$$

Substituting the flowfield, eliminating the remaining derivatives and collecting by node, we get

$$\left\{\left[\frac{\kappa\sin\left(\pi r^2\right)}{2\Delta r}-\frac{r}{Re\left(\Delta r\right)^2}-\frac{1}{Re}\frac{1}{2\Delta r}\right]u_\theta\right\}^{i-1}$$

$$+\left\{\begin{array}{l}\left(\dfrac{\pi\kappa Rere^{-\pi\kappa Rer^2/2}}{1-e^{-\pi\kappa Re/2}}-\dfrac{2iq}{rRe}\right)u_r+\left[\begin{array}{l}-i\omega r+iq\dfrac{1-e^{-\pi\kappa Rer^2/2}}{r\left(1-e^{-\pi\kappa Re/2}\right)}+\dfrac{1}{Re}\left(\dfrac{1+q^2}{r}+r\sigma^2\right)\\ +2\kappa\pi r\left(1+i\sigma z\right)\cos\left(\pi r^2\right)+\dfrac{2r}{Re\left(\Delta r\right)^2}\end{array}\right]u_\theta\\ +0u_z+iqp\end{array}\right\}^i$$

$$+\left\{\left[-\frac{\kappa\sin\left(\pi r^2\right)}{2\Delta r}-\frac{r}{Re\left(\Delta r\right)^2}+\frac{1}{Re}\frac{1}{2\Delta r}\right]u_\theta\right\}^{i+1}=0 \tag{42}$$

z-Momentum:

We remove the singularity at the centerline by multiplying by *r*:

$$r\frac{\partial U_z}{\partial r}u_r+0u_\theta+\left[-i\omega r+iqU_\theta+i\sigma rU_z+r\frac{\partial U_z}{\partial z}+\frac{1}{Re}\left(\frac{q^2}{r}+\sigma^2 r\right)\right]u_z+i\sigma rp+\left(rU_r-\frac{1}{Re}\right)\frac{\partial u_z}{\partial r}-\frac{r}{Re}\frac{\partial^2 u_z}{\partial r^2}=0 \tag{43}$$

This is followed by the use of the 2nd order Taylor series expansion with variable coefficients:

$$\left(r\frac{\partial U_z}{\partial r}u_r\right)^i+0u_\theta+\left\{\left[-i\omega r+iqU_\theta+i\sigma rU_z+r\frac{\partial U_z}{\partial z}+\frac{1}{Re}\left(\frac{q^2}{r}+\sigma^2 r\right)\right]u_z\right\}^i+\left(i\sigma rp\right)^i$$

$$+\frac{\Delta_{i-1}^{i+1}}{2\Delta r}\left[\left(rU_r-\frac{1}{Re}\right)u_z\right]-\left[\frac{\partial}{\partial r}\left(rU_r-\frac{1}{Re}\right)u_z\right]^i-\frac{1}{Re}\left\{\frac{\nabla_{i-1}^{i+1}}{(\Delta r)^2}(ru_z)+\left[\frac{\mathrm{d}^2}{\mathrm{d}r^2}(r)u_z\right]^i-2\frac{\Delta_{i-1}^{i+1}}{2\Delta r}\left[\frac{\mathrm{d}}{\mathrm{d}r}(r)u_z\right]\right\}=0 \qquad (44)$$

Substituting the flowfield, eliminating the remaining derivatives, and collecting by node, we get

$$\left\{\left[\frac{\kappa\sin\left(\pi r^2\right)}{2\Delta r}-\frac{r}{Re(\Delta r)^2}-\frac{1}{2Re\Delta r}\right]u_z\right\}^{i-1}$$

$$+\left\{-4\pi^2\kappa z r^2\sin\left(\pi r^2\right)u_r+0u_\theta+\left[\begin{array}{l}-i\omega r+iq\dfrac{1-e^{-\pi\kappa Re r^2/2}}{r\left(1-e^{-\pi\kappa Re/2}\right)}+2\left(2+i\sigma z\right)\pi\kappa r\cos\left(\pi r^2\right)\\+\dfrac{1}{Re}\left(\dfrac{q^2}{r}+\sigma^2 r\right)+\dfrac{2r}{(\Delta r)^2 Re}\end{array}\right]u_z+i\sigma r p\right\}^i$$

$$+\left\{\left[-\frac{\kappa\sin\left(\pi r^2\right)}{2\Delta r}-\frac{r}{(\Delta r)^2 Re}+\frac{1}{2Re\Delta r}\right]u_z\right\}^{i+1}=0 \qquad (45)$$

The system of equations for the interior nodes becomes:

$$AZ^{i-1}+BZ^i+CZ^{i+1}=\omega DZ^i \qquad (46)$$

where

$$Z^i=\left[u_r \quad u_\theta \quad u_z \quad p\right]^i \qquad (47)$$

and

$$A=\left[\begin{array}{cccc}\dfrac{1}{2\Delta r}\left[\kappa\sin\left(\pi r^2\right)-\dfrac{1}{Re}\right]-\dfrac{1}{Re}\dfrac{r}{(\Delta r)^2} & 0 & 0 & -\dfrac{r}{2\Delta r}\\ 0 & \dfrac{1}{2\Delta r}\left[\kappa\sin\left(\pi r^2\right)-\dfrac{1}{Re}\right]-\dfrac{1}{Re}\dfrac{r}{(\Delta r)^2} & 0 & 0\\ 0 & 0 & \dfrac{1}{2\Delta r}\left[\kappa\sin\left(\pi r^2\right)-\dfrac{1}{Re}\right]-\dfrac{1}{Re}\dfrac{r}{(\Delta r)^2} & 0\\ -\dfrac{r}{2\Delta r} & 0 & 0 & 0\end{array}\right]^{i-1} \qquad (48)$$

$$B=\begin{bmatrix}
\left\{\begin{array}{l}\dfrac{\kappa}{r}\sin\left(\pi r^2\right)+iq\dfrac{1-e^{-\pi\kappa Rer^2/2}}{r\left(1-e^{-\pi\kappa Re/2}\right)}\\ +2i\sigma r\pi\kappa z\cos\left(\pi r^2\right)\\ +\dfrac{1}{Re}\left[\dfrac{1+q^2}{r}+r\sigma^2+\dfrac{2r}{(\Delta r)^2}\right]\end{array}\right\} & 2\left[\dfrac{iq}{rRe}-\dfrac{1-e^{-\pi\kappa Rer^2/2}}{r\left(1-e^{-\pi\kappa Re/2}\right)}\right] & 0 & -1 \\
\dfrac{\pi\kappa Ree^{-\pi\kappa Rer^2/2}}{1-e^{-\pi\kappa Re/2}}r-\dfrac{2iq}{rRe} & \left\{\begin{array}{l}iq\dfrac{1-e^{-\pi\kappa Rer^2/2}}{r\left(1-e^{-\pi\kappa Re/2}\right)}\\ +2\kappa\pi r\left(1+i\sigma z\right)\cos\left(\pi r^2\right)\\ +\dfrac{1}{Re}\left[\dfrac{1+q^2}{r}+r\sigma^2+\dfrac{2r}{(\Delta r)^2}\right]\end{array}\right\} & 0 & iq \\
-4\pi^2\kappa zr^2\sin\left(\pi r^2\right) & 0 & \left\{\begin{array}{l}\kappa\sin\left(\pi r^2\right)\\ +iq\dfrac{1-e^{-\pi\kappa Rer^2/2}}{r\left(1-e^{-\pi\kappa Re/2}\right)}\\ +2\left(2+i\sigma z\right)\pi\kappa r\cos\left(\pi r^2\right)\\ +\dfrac{1}{Re}\left[\dfrac{q^2}{r}+\sigma^2 r+\dfrac{2r}{(\Delta r)^2}\right]\end{array}\right\} & i\sigma r \\
0 & iq & i\sigma r & 0
\end{bmatrix}^i \tag{49}$$

$$C=\begin{bmatrix}
\dfrac{1}{2\Delta r}\left[\dfrac{1}{Re}-\kappa\sin\left(\pi r^2\right)\right]-\dfrac{r}{Re(\Delta r)^2} & 0 & 0 & \dfrac{r}{2\Delta r} \\
0 & \dfrac{1}{2\Delta r}\left[\dfrac{1}{Re}-\kappa\sin\left(\pi r^2\right)\right]-\dfrac{r}{Re(\Delta r)^2} & 0 & 0 \\
0 & 0 & \dfrac{1}{2\Delta r}\left[\dfrac{1}{Re}-\kappa\sin\left(\pi r^2\right)\right]-\dfrac{r}{Re(\Delta r)^2} & 0 \\
\dfrac{r}{2\Delta r} & 0 & 0 & 0
\end{bmatrix}^{i+1} \tag{50}$$

and, finally,

$$D=\begin{bmatrix}ir & 0 & 0 & 0\\ 0 & ir & 0 & 0\\ 0 & 0 & ir & 0\\ 0 & 0 & 0 & 0\end{bmatrix}^i \tag{51}$$

It may be worthwhile to mention that our boundary conditions were also adopted by Abu-Irshaid, Majdalani and Casalis.[56] At the outer radius, we just set the derivative of the perturbed pressure to zero (a natural Neumann-type condition). The "hardwall" Dirichlet boundary conditions for the perturbed velocity require no extra work, as the values are fixed to zero. We have

$$u_r(1) = u_\theta(1) = u_z(1) = \frac{\partial p}{\partial r}(1) = 0 \tag{52}$$

Note that in previous studies,[58] the pressure is set equal to one at the wall. This acts to normalize the amplitude of the solution, and was necessary for the shooting approach. However, the eigensolver does not allow for nonzero fixed boundary values, so we permit the pressure amplitude to float by setting the derivative of the pressure to zero.

Applying the outer radial boundary conditions, using a two point backwards difference, yields:

$$Z^N = [p] \qquad C^{N-1} = \begin{bmatrix} \frac{r}{2\Delta r} \\ 0 \\ 0 \\ 0 \end{bmatrix}^N \qquad A^N = [0 \quad 0 \quad 0 \quad -1] \qquad B^N = [1] \qquad D^N = [0] \tag{53}$$

It may be useful to mention that we have also used a three-point, second-order backwards difference equation with nearly identical results to those obtained above.

Concerning the centerline boundary conditions, they remain a function of q, namely,

$$\begin{aligned} q = 0: &\quad u_r(0) = u_\theta(0) = \frac{\partial u_z}{\partial r}(0) = \frac{\partial p}{\partial r}(0) = 0 \\ q = 1: &\quad \frac{\partial u_r}{\partial r}(0) = \frac{\partial u_\theta}{\partial r}(0) = u_z(0) = p(0) = 0 \\ q \geq 2: &\quad u_r(0) = u_\theta(0) = u_z(0) = p(0) = 0 \end{aligned} \tag{54}$$

Thus, for $q = 0$, one collects

$$Z^1 = [u_z \quad p]^T \tag{55}$$

Two approaches were used, and they yielded nearly identical results. In both cases, the perturbed pressure derivative was set to zero using a three-point Taylor series expansion. In the first case, the perturbed axial velocity was related to the perturbed pressure using the axial momentum equation:

$$\frac{\partial U_z}{\partial r} u_r + 0 u_\theta + \left[-i\omega + \frac{iqU_\theta}{r} + i\sigma U_z + \frac{\partial U_z}{\partial z} + \frac{1}{Re}\left(\frac{q^2}{r^2} + \sigma^2 \right) \right] u_z + i\sigma p + \left(U_r - \frac{1}{Re}\frac{1}{r} \right) \frac{\partial u_z}{\partial r} - \frac{1}{Re}\frac{\partial^2 u_z}{\partial r^2} = 0 \tag{56}$$

$$\left(-i\omega + i\sigma U_z + \frac{\partial U_z}{\partial z} + \frac{\sigma^2}{Re} \right) u_z^0 + i\sigma p_z^0 - \frac{1}{Re(\Delta r)^2}\left(u_z^{+1} - 2u_z^0 + u_z^{-1} \right) = 0 \tag{57}$$

$$\frac{\partial u_z}{\partial r} = 0 \Rightarrow u_z^{-1} = u_z^{+1} \tag{58}$$

$$\left(-i\omega + i\sigma U_z + \frac{\partial U_z}{\partial z} + \frac{\sigma^2}{Re} \right) u_z^0 + i\sigma p_z^0 - \frac{2}{Re(\Delta r)^2}\left(u_z^{+1} - u_z^0 \right) = 0 \tag{59}$$

$$\left[-i\omega + i\sigma U_z + \frac{\partial U_z}{\partial z} + \frac{\sigma^2}{Re} + \frac{2}{Re(\Delta r)^2} \right] u_z^0 + i\sigma p_z^0 - \frac{2}{Re(\Delta r)^2} u_z^{+1} = 0 \tag{60}$$

$$\left[-i\omega+2i\sigma\pi\kappa z\cos\left(\pi r^2\right)+2\pi\kappa\cos\left(\pi r^2\right)+\frac{\sigma^2}{Re}+\frac{2}{Re\left(\Delta r\right)^2}\right]u_z^0+i\sigma p_z^0-\frac{2}{Re\left(\Delta r\right)^2}u_z^{+1}=0 \tag{61}$$

$$\left[-i\omega+2\left(1+i\sigma z\right)\pi\kappa\cos\left(\pi r^2\right)+\frac{\sigma^2}{Re}+\frac{2}{Re\left(\Delta r\right)^2}\right]u_z^0+i\sigma p_z^0-\frac{2}{Re\left(\Delta r\right)^2}u_z^{+1}=0 \tag{62}$$

$$\left[-i\omega+2\left(1+i\sigma z\right)\pi\kappa+\frac{\sigma^2}{Re}+\frac{2}{Re\left(\Delta r\right)^2}\right]u_z^0+i\sigma p_z^0-\frac{2}{Re\left(\Delta r\right)^2}u_z^{+1}=0 \tag{63}$$

For this situation, the boundary conditions become:

$$A^2=\begin{bmatrix}0 & -\frac{r}{2\Delta r}\\ 0 & 0\\ \frac{1}{2\Delta r}\left[\kappa\sin\left(\pi r^2\right)-\frac{1}{Re}\right]-\frac{1}{Re}\frac{r}{\left(\Delta r\right)^2} & 0\\ 0 & 0\end{bmatrix}^1 \tag{64}$$

$$B^1=\begin{bmatrix}2\left(1+i\sigma z\right)\pi\kappa+\frac{\sigma^2}{Re}+\frac{2}{Re\left(\Delta r\right)^2} & i\sigma\\ 0 & -1\end{bmatrix} \tag{65}$$

$$C^1=\begin{bmatrix}0 & 0 & -\frac{2}{Re\left(\Delta r\right)^2} & 0\\ 0 & 0 & 0 & 1\end{bmatrix} \tag{66}$$

$$D^1=\begin{bmatrix}-i & 0\\ 0 & 0\end{bmatrix} \tag{67}$$

Alternately, it is possible to merely set the derivative of the axial velocity to zero using a three-point Taylor series expansion. However, we find that results obtained from both approaches are virtually identical.

For the first azimuthal mode number, $q = 1$, one obtains

$$q=1:\quad \frac{\partial u_r}{\partial r}(0)=\frac{\partial u_\theta}{\partial r}(0)=u_z\left(0\right)=p(0)=0 \tag{68}$$

$$Z^1=\begin{bmatrix}u_r & u_\theta\end{bmatrix}^T \tag{69}$$

In this case, two-point differences are used to set the boundary derivatives to zero. One finds

$$A^2=\begin{bmatrix}\frac{r}{2\Delta r}\left[\kappa r\sin\left(\pi r^2\right)-\frac{3}{Re}\right]-\frac{1}{\mathrm{Re}}\frac{r^2}{\left(\Delta r\right)^2} & 0\\ 0 & \frac{r}{2\Delta r}\left[\kappa r\sin\left(\pi r^2\right)-\frac{3}{Re}\right]-\frac{1}{Re}\frac{r^2}{\left(\Delta r\right)^2}\\ 0 & 0\\ -\frac{r}{2\Delta r} & 0\end{bmatrix}^1 \tag{70}$$

$$B^1 = \begin{bmatrix} -1 & 0 \\ 0 & -1 \end{bmatrix} \qquad C^1 = \begin{bmatrix} 1 & 0 & 0 & 0 \\ 0 & 1 & 0 & 0 \end{bmatrix} \qquad D^1 = \begin{bmatrix} 0 & 0 \\ 0 & 0 \end{bmatrix} \tag{71}$$

Finally, for $q \geq 2$, one is left with

$$q \geq 2: \quad u_r(0) = u_\theta(0) = u_z(0) = p(0) = 0 \tag{72}$$

Given all Dirichlet boundary conditions, we do not need A^2, B^1 or C^1.

Before making further headway, it may be useful to recall that a typical eigenvalue problem takes the form:

$$A_{ij} x_j = \lambda x_i \tag{73}$$

Unfortunately, this relation does not fit the problem at hand. Continuity provides an inherent constraint that must be maintained, and does not have an eigenvalue parameter ω to fit the form of Eq. (73). Momentum has an additional variable, the pressure, that does not have an eigenvalue associated with it. The continuity constraint becomes the extra equation that is needed to account for the fourth variable (pressure). Fortunately, ARPACK can solve the most general eigenvalue problem with complex eigenvalues and eigenvectors, for non-symmetric matrices.

$$A_{ij} x_j = \lambda M_{ij} x_j \tag{74}$$

Note that Eq. (74) reverts to the previous form given by Eq. (73) in the case of M_{ij} being the identity matrix. This form is reminiscent of the system of equations that we define here through Eq. (46). Interestingly, ARPACK allows M_{ij} to be singular,[55] which would correlate to this paper's D matrix, Eq. (51). We take advantage of this behavior to impose the continuity constraint in lieu of the eigenvalue row associated with the pressure, as in the lower rows of the A, B and C matrices, Eqs. (48), (49) and (50). This approach enforces the irrotational condition and solves for the pressure in terms of the velocity field.

According to the ARPACK User Guide,[58] one must factorize the matrix to compute the inverse:

$$I = (A - \sigma M)^{-1} \tag{75}$$

As this matrix is used in a repeated matrix-vector dot product (as part of the solution iteration process), it is helpful to store the factorization. The σ parameter is introduced to help the user specify an initial value to search about for eigenvalues. In our program, we set this value to zero, as normally the lowest real eigenvalues are associated with the most unstable modes.

IV. Results

We attempted to match the results of Table II in Abu-Irshaid, Majdalani and Casalis,[58] which contained the temporal eigenmodes as a function of the spatial eigenmodes. However, the eigenmodes we obtained were different. We obtained four complex modes for the system of equations that are shown in Table 1 (z = 10, q = 0, Re = 5000, κ = 0.1). In doing so, we discovered that when q = 0, the tangential momentum equation, containing only the tangential velocity and being the only place where the tangential velocity appears, becomes independent of the other three equations. As such, it must be removed from the set of equations lest it corrupts the eigenvalue computation. It is possible that we merely found different modes than those found previously or that the two approaches are essentially dissimilar:[55]

Table 1. Prediction for the vortex chamber at z = 10, q = 0, and Re = 5,000

Mode	ω_r	ω_i
1	0.04351	0.14414
2	0.05756	0.10101
3	0.05770	0.07379
4	0.03464	0.07108

Given the eigenvalues in Table 1, it is possible to plot the mode shapes for each hydrodynamic variable. To this end, the perturbed velocities (radial, tangential, and axial) and the pressure are plotted in Figure 1 for the first mode in Table 1.

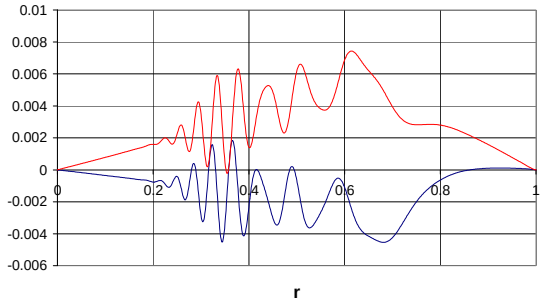

a) Perturbed radial velocity

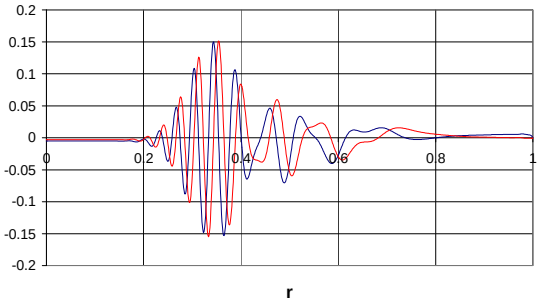

b) Perturbed axial velocity

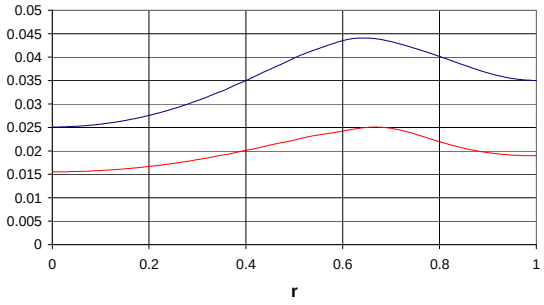

c) Perturbed pressure

Figure 1. Perturbed flow field for first mode in Table 1. Blue and red lines denote real and imaginary parts.

V. Conclusions

Herein a system of equations defining the hydrodynamic eigenvalue problem as a perturbation of the Euler equations is presented. An analytic mean flowfield, which represents the motion of a bidirectional vortex is introduced into the system of equations. As a result, the spatially variable coefficients that control the perturbation equations are identified. Second-order, two-parameter central differences, based on Taylor series expansions, are used to account for the spatial variations. As the continuity equation is independent of time, it does not contain the temporal frequency. This causes the overall system of equations to exhibit a positive, semi-definite, but singular portion. By using a shift-invert technique, the ARPACK eigensolver code is used to overcome this problem and solve for the complex eigenvalues and eigenmodes. The new eigensolver is quite general as it can handle non-symmetric matrices and matrices with singularities.

VI. Future Efforts

One goal of turning this problem into a finite difference system of linear equations, instead of the LNP approach used previously,[58] is to demonstrate the potential capability to extend the analysis to three dimensions. While this will greatly increase the computational requirements, the boundary conditions will be simplified as the no-slip boundary will apply to all surfaces, and special centerline boundary conditions will no longer be needed. It will still be necessary to force the normal pressure derivative to be zero, but this may be overcome using a finite volume discretization technique. It is also important to determine the origin of the differences with the LNP prediction. The disparities could be due to human error, or to the generally dissimilar approach and boundary conditions associated with the present model. In forthcoming work, we intend to incorporate other mean and perturbed flowfield phenomena, including the effect of particle-mean flow interactions.

Acknowledgments

This work is sponsored by the National Science Foundation through STTR Phase I Grant No. CMS-0611362.

References

[1]Chedevergne, F., Casalis, G., and Majdalani, J., "Biglobal Linear Stability Analysis and DNS Investigation of the Flow Induced by Wall Injection," AIAA Paper 2007-5796, July 2007.

[2]Chedevergne, F., and Casalis, G., "Thrust Oscillations in Reduced Scale Solid Rocket Motors, Part II : A New Theoretical Approach," AIAA Paper 2005-4000, July 2005.

[3]Chedevergne, F., Casalis, G., and Féraille, T., "Biglobal Linear Stability Analysis of the Flow Induced by Wall Injection," *Physics of Fluids,* Vol. 18, No. 1, 2006, pp. 014103-14.

[4]Chedevergne, F., and Casalis, G., "Detailed Analysis of the Thrust Oscillations in Reduced Scale Solid Rocket Motors," AIAA Paper 2006-4424, July 2006.

[5]Abu-Irshaid, E. M., Majdalani, J., and Casalis, G., "Stability of Rockets with Headwall Injection," AIAA Paper 2005-3543, July 2005.

[6]Bhatia, L., Abu-Irshaid, E. M., Majdalani, J., and Casalis, G., "Stability of the Taylor-Culick Profile with Headwall Injection and Particle Interactions," AIAA Paper 2006-4429, July 2006.

[7]Flandro, G. A., Majdalani, J., and French, J. C., "Incorporation of Nonlinear Capabilities in the Standard Stability Prediction Program," AIAA Paper 2004-4182, July 2004.

[8]Flandro, G. A., Fischbach, S. R., Majdalani, J., and French, J. C., "Nonlinear Rocket Motor Stability Prediction: Limit Amplitude, Triggering, and Mean Pressure Shift," AIAA Paper 2004-4054, July 2004.

[9]Griffond, J., and Casalis, G., "On the Nonparallel Stability of the Injection Induced Two-Dimensional Taylor Flow," *Physics of Fluids,* Vol. 13, No. 6, 2001, pp. 1635-1644.

[10]Griffond, J., and Casalis, G., "On the Dependence on the Formulation of Some Nonparallel Stability Approaches Applied to the Taylor Flow," *Physics of Fluids,* Vol. 12, No. 2, 2000, pp. 466-468.

[11]Griffond, J., "Receptivity and Aeroacoustic Resonance in Channels with Blowing Walls," *Physics of Fluids,* Vol. 14, No. 11, 2002, pp. 3946-3962.

[12]Féraille, T., and Casalis, G., "Channel Flow Induced by Wall Injection of Fluid and Particles," *Physics of Fluids,* Vol. 15, No. 2, 2003, pp. 348-360.

[13]Fischbach, S. R., Majdalani, J., and Flandro, G. A., "Acoustic Instability of the Slab Rocket Motor," *Journal of Propulsion and Power,* Vol. 23, No. 1, 2007, pp. 146-157.

[14]Fischbach, S. R., Majdalani, J., and Flandro, G. A., "Verification and Validation of Rocket Stability Integral Transformations," AIAA Paper 2005-4001, July 2005.

[15]Fischbach, S. R., Majdalani, J., and Flandro, G. A., "Acoustic Instability of the Slab Rocket Motor," AIAA Paper 2004-4061, July 2004.

[16]Fischbach, S. R., Flandro, G. A., and Majdalani, J., "Volume-to-Surface Transformations of Rocket Stability Integrals," AIAA Paper 2004-4053, July 2004.

[17]Flandro, G. A., and Majdalani, J., "Aeroacoustic Instability in Rockets," *AIAA Journal,* Vol. 41, No. 3, 2003, pp. 485-497.

[18]Majdalani, J., Fischbach, S. R., and Flandro, G. A., "Improved Energy Normalization Function in Rocket Motor Stability Calculations," *Journal of Aerospace Science and Technology,* Vol. 10, No. 6, 2006, pp. 495-500.

[19]Majdalani, J., Flandro, G. A., and Fischbach, S. R., "Some Rotational Corrections to the Acoustic Energy Equation in Injection-Driven Enclosures," *Physics of Fluids,* Vol. 17, No. 7, 2005, pp. 0741021-20.

[20]Majdalani, J., "Physicality of Core Flow Models in Rocket Motors," *Journal of Propulsion and Power,* Vol. 19, No. 1, 2003, pp. 156-159.

[21]Majdalani, J., and Flandro, G. A., "The Oscillatory Pipe Flow with Arbitrary Wall Injection," *Proceedings of the Royal Society, London, Series A,* Vol. 458, No. 2022, 2002, pp. 1621-1651.

[22]Majdalani, J., Barron, J., and Van Moorhem, W. K., "Inception of Turbulence in the Stokes Boundary Layer over a Transpiring Wall," *ASME Journal of Fluids Engineering,* Vol. 124, No. 9, 2002, pp. 1-7.

[23]Majdalani, J., and Van Moorhem, W. K., "Laminar Cold-Flow Model for the Internal Gas Dynamics of a Slab Rocket Motor," *Journal of Aerospace Science and Technology,* Vol. 5, No. 3, 2001, pp. 193-207.

[24]Majdalani, J., "Improved Solution for the Vortical and Acoustical Mode Coupling inside a Two-Dimensional Cavity with Porous Walls," *Journal of the Acoustical Society of America,* Vol. 109, No. 2, 2001, pp. 475-479.

[25]Majdalani, J., "The Oscillatory Channel Flow with Arbitrary Wall Injection," *Journal of Applied Mathematics and Physics (ZAMP),* Vol. 52, No. 1, 2001, pp. 33-61.

[26]Majdalani, J., and Roh, T. S., "The Oscillatory Channel Flow with Large Wall Injection," *Proceedings of the Royal Society, London, Series A,* Vol. 456, No. 1999, 2000, pp. 1625-1657.

[27]Barron, J., Majdalani, J., and Van Moorhem, W. K., "A Novel Investigation of the Oscillatory Field over a Transpiring Surface," *Journal of Sound and Vibration,* Vol. 235, No. 2, 2000, pp. 281-297.

[28]Majdalani, J., "The Boundary Layer Structure in Cylindrical Rocket Motors," *AIAA Journal,* Vol. 37, No. 4, 1999, pp. 505-508.

[29]Majdalani, J., and Van Moorhem, W. K., "Improved Time-Dependent Flowfield Solution for Solid Rocket Motors," *AIAA Journal,* Vol. 36, No. 2, 1998, pp. 241-248.

[30]Balachandar, S., Buckmaster, J. D., and Short, M., "The Generation of Axial Vorticity in Solid-Propellant Rocket-Motor Flows," *Journal of Fluid Mechanics,* Vol. 429, No. 1, 2001, pp. 283-305.

[31]Wasistho, B., Balachandar, S., and Moser, R. D., "Compressible Wall-Injection Flows in Laminar, Transitional, and Turbulent Regimes: Numerical Prediction," *Journal of Spacecraft and Rockets,* Vol. 41, No. 6, 2004, pp. 915-924.

[32]Kirkköprü, K., Kassoy, D. R., and Zhao, Q., "Unsteady Vorticity Generation and Evolution in a Model of a Solid Rocket Motor," *Journal of Propulsion and Power,* Vol. 12, No. 4, 1996, pp. 646-654.

[33]Staab, P. L., and Kassoy, D. R., "Three-Dimensional, Unsteady, Acoustic-Shear Flow Dynamics in a Cylinder with Sidewall Mass Addition," *Physics of Fluids, Series B,* Vol. 9, 1996, pp. 3753-3763.

[34]Zhao, Q., Staab, P. L., Kassoy, D. R., and Kirkköprü, K., "Acoustically Generated Vorticity in an Internal Flow," *Journal of Fluid Mechanics,* Vol. 413, No. 1, 2000, pp. 247-285.

[35]French, J. C., "Tangential Mode Instability of SRMs with Even and Odd Numbers of Slots," AIAA Paper 2002-3612, July 2002.

[36]French, J. C., Flandro, G. A., and Majdalani, J., "Improvements to the Linear Standard Stability Prediction Program (SSP)," AIAA Paper 2004-4181, July 2004.

[37]French, J. C., and Flandro, G. A., "Linked Solid Rocket Motor Combustion Stability and Internal Ballistics Analysis," AIAA Paper 2005-3998, July 2005.

[38]French, J. C., and Coats, D. E., "Automated 3-D Solid Rocket Combustion Stability Analysis," AIAA Paper 99-2797, June 1999.

[39]Couton, D., Plourde, F., and Doan-Kim, S., "Cold Gas Simulation of a Solid Propellant Rocket Motor," *AIAA Journal,* Vol. 34, No. 12, 1996, pp. 2514-2522.

[40]Varapaev, V. N., and Yagodkin, V. I., "Flow Stability in a Channel with Porous Walls," *Fluid Dynamics (Izvestiya Akademii Nauk SSSR, Meckanika Zhidkosti i Gaza),* Vol. 4, No. 5, 1969, pp. 91-95.

[41]Beddini, R. A., "Injection-Induced Flows in Porous-Walled Ducts," *AIAA Journal,* Vol. 24, No. 11, 1986, pp. 1766-1773.

[42]Beddini, R. A., and Roberts, T. A., "Turbularization of an Acoustic Boundary Layer on a Transpiring Surface," *AIAA Journal,* Vol. 26, No. 8, 1988, pp. 917-923.

[43]Beddini, R. A., and Roberts, T. A., "Response of Propellant Combustion to a Turbulent Acoustic Boundary Layer," *Journal of Propulsion and Power,* Vol. 8, No. 2, 1992, pp. 290-296.

[44]Lee, Y., and Beddini, R. A., "Acoustically-Induced Turbulent Transition in Solid Propellant Rocket Chamber Flowfields," AIAA Paper 99-2508, June 1999.

[45]Lee, Y., and Beddini, R. A., "Effect of Solid Rocket Chamber Pressure on Acoustically-Induced Turbulent Transition," AIAA Paper 2000-3802, July 2000.

[46]Casalis, G., Avalon, G., and Pineau, J.-P., "Spatial Instability of Planar Channel Flow with Fluid Injection through Porous Walls," *Physics of Fluids,* Vol. 10, No. 10, 1998, pp. 2558-2568.

[47]Avalon, G., and Comas, P., "Simulative Study of the Unsteady Flow inside a Solid Propellant Rocket Motor," AIAA Paper 91-1866, June 1991.

[48]Vuillot, F., and Avalon, G., "Acoustic Boundary Layer in Large Solid Propellant Rocket Motors Using Navier-Stokes Equations," *Journal of Propulsion and Power,* Vol. 7, No. 2, 1991, pp. 231-239.

[49]Vuillot, F., "Vortex-Shedding Phenomena in Solid Rocket Motors," *Journal of Propulsion and Power,* Vol. 11, No. 4, 1995, pp. 626-639.

[50]Couton, D., Doan-Kim, S., and Vuillot, F., "Numerical Simulation of Vortex-Shedding Phenomenon in a Channel with Flow Induced through Porous Wall," *International Journal of Heat and Fluid Flow,* Vol. 18, No. 3, 1997, pp. 283-296.

[51]Ugurtas, B., Avalon, G., Lupoglazoff, N., and Vuillot, F., "Numerical Computations of Hydrodynamic Instabilities inside Channels with Wall Injection," AIAA Paper 99-2505, June 1999.

[52]Avalon, G., Casalis, G., and Griffond, J., "Flow Instabilities and Acoustic Resonance of Channels with Wall Injection," AIAA Paper 98-3218, July 1998.

[53]Ugurtas, B., Avalon, G., Lupoglazoff, N., Vuillot, F., and Casalis, G., "Stability and Acoustic Resonance of Internal Flows Generated by Side Injection," *Solid Propellant Chemistry, Combustion, and Motor Interior Ballistics*, Vol. 185, edited by V. Yang, T. B. Brill, and W.-Z. Ren, AIAA Progress in Astronautics and Aeronautics, Washington, DC, 2000, pp. 823-836.

[54]Fabignon, Y., Dupays, J., Avalon, G., Vuillot, F., Lupoglazoff, N., Casalis, G., and Prévost, M., "Instabilities and Pressure Oscillations in Solid Rocket Motors," *Journal of Aerospace Science and Technology*, Vol. 7, No. 3, 2003, pp. 191-200.

[55]Lehoucq, R. B., Sorensen, D. C., and Yang, C., *ARPACK Users Guide: Solution of Large Scale Eigenvalue Problems with Implicitly Restarted Arnoldi Methods*, Rice University, Houston, TX, 1997.

[56]Abu-Irshaid, E. M., Majdalani, J., and Casalis, G., "Hydrodynamic Stability of Rockets with Headwall Injection," *Physics of Fluids*, Vol. 19, No. 2, 2007, pp. 024101-11.

[57]Vyas, A. B., Majdalani, J., and Chiaverini, M. J., "The Bidirectional Vortex. Part 2: Viscous Core Corrections," AIAA Paper 2003-5053, July 2003.

[58]Abu-Irshaid, E. M., Majdalani, J., and Casalis, G., "Hydrodynamic Instability of the Bidirectional Vortex," AIAA Paper 2005-4531, July 2005.